# Passive Control Design for Multi-terminal VSC-HVDC Systems via Energy Shaping

B. Yang[1], L. Jiang[2], Tao Yu[3], H. C. Shu[1], Chuan-Ke Zhang[5], Wei Yao*[6], and Q. H. Wu[3]

[1]*Faculty of Electric Power Engineering, Kunming University of Science and Technology, Kunming 650500, China*

[2]*Department of Electrical Engineering and Electronics, University of Liverpool, Liverpool, L69 3GJ, United Kingdom*

[3]*School of Electrical Engineering, South China University of Technology, Guangzhou, Guangdong, 510641, China*

[4]*Department of Electrical Engineering and Electronics, University of Liverpool, Liverpool, L69 3GJ, United Kingdom*

[5]*School of Automation, China University of Geosciences, Wuhan 430074, China*

[6]*State Key Laboratory of Advanced Electromagnetic Engineering and Technology, School of Electrical and Electronic Engineering, Huazhong University of Science and Technology, Wuhan, 430074, China*

**Abstract**

This paper investigates a passive control (PC) scheme for multi-terminal voltage source converter (VSC) based high voltage direct current (VSC-HVDC) systems, which can provide a reliable and effective integration of electrical power from renewable energy. A storage function is constructed for each terminal and reshaped into a desired output strictly passive form via feedback passivation with an extra system damping. The beneficial nonlinearities are retained which results in a better transient dynamics of the active power, reactive power, and direct current cable voltage. Then the retained internal dynamics related to the direct current (DC) cable current and common DC voltage is proved to be asymptotically stable by zero-dynamics technique of output dynamics, thus the closed-loop system can be asymptotically stabilized. Case studies are carried out on a four-terminal VSC-HVDC system, under six conditions, e.g., active power and reactive power regulation with parameter uncertainties, faults at alternating current (AC) bus and DC cable, offshore wind farm connection, weak AC grid connection, and robustness of DC cable resistance uncertainties. Simulation results verify the effectiveness of PC against that of linear proportional-integral (PI) control and nonlinear feedback linearization control (FLC) under various operation conditions.

*Corresponding Author: w.yao@hust.edu.cn

# 1 Introduction

In the past decades, the ever-increasing penetration of renewable energy (wind, solar, wave, hydro, and biomass) requires an extraordinarily reliable and effective transmission of electrical power from these new sources to the main power grid, in which hydro power has already been fully exploited in many grids, such that a sustainable development can be achieved in future [1]. The problems and perspectives of converting present energy systems (mainly thermal and nuclear) into a 100% renewable energy system has been discussed with a conclusion that such idea is possible, which however raises that advanced transmission technologies are needed to realize this goal [2].

The need for more secure power grids and increasing environmental concerns continue to drive the worldwide deployment of high voltage direct current (HVDC) transmission technology. HVDC systems use power electronic devices to convert alternative current (AC) into direct current (DC), they are an economical way of transmitting bulk electrical power in DC over long distance overhead line or short submarine cable, while advanced extruded DC cable technologies have been used to increase power transmissions by at least 50 percent [3, 4], which is also an important onshore solution. HVDC enables secure and stable asynchronous interconnection of power networks that operate on different frequencies. Different technologies have

been used to design two-terminal HVDC systems for the purpose of a point-to-point power transfer, such as line-commutated converter (LCC) based HVDC (LCC-HVDC) systems using grid-controlled mercury-arc valves or thyristors, capacitor-commutated converter (CCC) based HVDC (CCC-HVDC) systems or controlled series commutated converter (CSCC) based HVDC (CSCC-HVDC) systems [5, 6].

Recently, multi-terminal HVDC systems are attracting tremendous attentions due to the requirement of power exchanges among multiple power suppliers and consumers, which can easily achieve power exchanges among multi-points, connection between asynchronous networks, and integration of scattered power plants like offshore renewable energy sources [7]. Though LCC converters can also be used for multi-terminal HVDC systems, e.g. Quebec-new England link, voltage source converters (VSC) are relatively easier to implement the control of parallel-connected multi-terminals systems [5]. Moreover, VSC-HVDC has many advantages over the LCC-HVDC system and has been proposed for integration of long distance large-scale onshore wind farms via overhead lines and offshore wind farms via submarine cables [8].

A large amount of researches has been devoted to design the control system for the VSC-HVDC, among which conventional vector control associated with proportional-integral (PI) loops is widely used. However its performance may be degraded when

operation conditions vary as its control parameters are determined by the one-point linearization of the original nonlinear system [9]. To tackle this issue, many advanced approaches are proposed, such as feedback linearization control (FLC) [10], multi-variable optimal control [11], feed-forward control [12], sliding mode control [13], feedback linearization based sliding mode control (FLSMC) [14], perturbation observer based sliding-mode control [15], and power-synchronization control [16]. Nevertheless, the aforementioned methods are merely developed for two-terminal VSC-HVDC systems. Recently, several controllers have also been designed for the multi-terminal VSC-HVDC system as well, such as adaptive parallel multi-PI controller [17], adaptive droop controller [18], wide area measurement system (WAMS) based controller [19], and perturbation observer based adaptive passive controller [20]. However, the above literatures haven't addressed the stability of the internal dynamics related to the DC cable current and common DC voltage during the control system design, which may cause an instability of the closed-loop system.

A passive system is characterized by the property that at any time the amount of energy which the system can conceivably supply to its environment cannot exceed the amount of energy that has been injected to it by external inputs. Passivity views a dynamical system as an energy-transformation device, which decomposes a complex nonlinear system into simpler subsystems that, upon interconnection, and

adds up their local energies to determine the full system's behaviour [21]. The action of a controller connected to the dynamical system may also be regarded, in terms of energy, as another separate dynamical system. Thus the control problem can then be treated as finding an interconnection pattern between the controller and the dynamical system, such that the changes of the overall storage function can take a desired form [22]. Compared to the one-point linearization based linear PI control, passive control (PC) carefully cancels the system nonlinearities, such that a globally consistent control performance can be achieved than that of PI control. Meanwhile, compared to FLC, PC retains the beneficial system nonlinearities instead of a full compensation, thus PC can enhance the system damping than that of FLC. The application of PC can be found in power system [23], doubly-fed induction machine [24], power converter [25], three-phase front end converter [26], and the integration of distributed generation (DG) [27].

Thus far, PC has been largely applied to VSC-HVDC systems. In terms of passivity, the power flow of alternating current (AC) networks into multi-terminal VSC-HVDC systems must be greater than or equal to the rate of change of the overall energies in multi-terminal VSC-HVDC systems, which are stored and exchangeable in the energy storage components such as capacitors and inductors [28]. An interconnection and damping assignment passivity-based (IDA-PB) control has

been applied based on the port-controlled Hamiltonian with dissipation (PCHD) model in [29] for a standard two-terminal VSC-HVDC system, which can provide more system damping than that of FLC [10] as the beneficial system nonlinearity is retained. However, it cannot be extended into multi-terminal VSC-HVDC systems as the internal dynamics cannot be represented and analyzed through the PCHD model.

In this paper, a PC has been developed for a multi-terminal VSC-HVDC system. A storage function, also known as the energy function, of the studied system is firstly constructed, then the energy shaping technique [21] is used as follows:

• Differentiate the storage function and carefully investigate the actual role of each term, then retain the beneficial ones while fully compensate all the others, such that the physical property of the multi-terminal VSC-HVDC system can be wisely exploited;

• Reshape the above system by transforming the previously manipulated storage function into an output strictly passive form of three controlled states: active power, reactive power, and DC cable voltage, via feedback passivation with an extra system damping, such that the transient responses of PC can be notably improved against that of the exact nonlinearity cancelation based FLC [10].

Moreover, the nonlinearities compensation of PC can provide a consistent control

performance under various operation points compared to that of the PI control [9]. Considering zero-dynamics of the active power, reactive power, and DC cable voltage, the retained internal dynamics related to the DC cable current and common DC voltage is proved to be asymptotically stable in the sense of Lyapunov criterion. The control performance of the PC is evaluated on a four-terminal VSC-HVDC system, in which its tracking performance of active and reactive power under parameter uncertainties is tested at first. Then its system dynamic enhancement is discussed under faults at AC bus and DC cable, offshore wind farm connections, weak AC grid connection, and robustness of DC cable resistance uncertainties, respectively. Simulation results are provided to demonstrate its superiority over the FLC and the PI control.

Section 2 presents the mathematical modelling of an $N$-terminal VSC-HVDC system. Section 3 develops the PC design for the $N$-terminal VSC-HVDC system. Simulation results on a four-terminal VSC-HVDC are given in Section 4. Some discussions about the application of PC into other situations and its benefit against PI control are made in Section 5. Finally, Section 6 concludes the paper.

# 2 Mathematical Modelling of an $N$-terminal VSC-HVDC System

The mathematical model of an $N$-terminal VSC-HVDC system is established in the synchronous $dq$ frame. A lumped parameter model is assumed and the AC network is represented through the series connection of the AC network voltage source and transmission line, which is interfaced to a VSC at the point of common coupling (PCC) shown in Fig. 1 through the transformer. $X_{\mathrm{d1}i}$ and $X_{\mathrm{d2}i}$ stand for the reactance of the short parallel transmission line [14] connecting between the AC network$_i$ and the corresponding PCC, which represents the external power network topology connected to the $N$-terminal VSC-HVDC system. Here, assume the AC networks are strong enough thus the reactance is ignored, e.g., $X_{\mathrm{d1}i} = X_{\mathrm{d2}i} = 0$ and $V_{\mathrm{s}i} = V_{\mathrm{s}i}^{'}$. A more detailed VSC model featuring the related switches can be employed but this would only add a slight ripple in the voltage waveforms due to the associated switching action, which does not significantly affect the fundamental dynamics [11], thus the VSCs are represented by their averaged model [18].

The phase-locked loop (PLL) is used during the transformation of the $abc$ frame to the $dq$ frame [30]. The $q$-axis is locked with the voltage $V_{\mathrm{s}i}$ on the AC side of the VSCs to ensure a decoupled control of the active power and reactive power. Only the

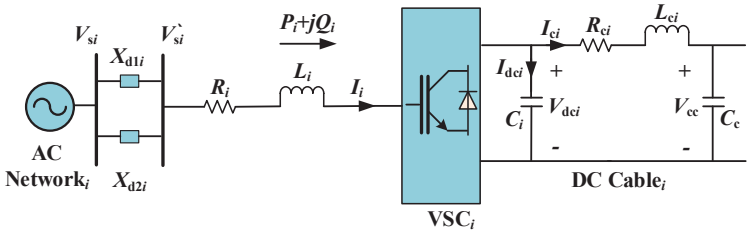


Figure 1: One terminal in an $N$-terminal VSC-HVDC system.

balanced condition is considered in this paper, i.e., the three phases have identical parameters and their voltages and currents have the same amplitude while each phase shifts 120° between themselves. Furthermore, it is assumed that the multi-terminal VSC-HVDC system is connected to sufficiently strong AC networks, in which the AC voltage remains as a constant. Lastly, the converter losses are neglected [10].

One terminal of an $N$-terminal VSC-HVDC system is illustrated in Fig. 1. On the AC side of the VSC station, the system dynamics can be expressed at the angular frequency $\omega_i$ as

$$\begin{cases} \dot{I}_{\mathrm{d}i} = -\frac{R_i}{L_i} I_{\mathrm{d}i} + \omega_i I_{\mathrm{q}i} + \frac{V_{\mathrm{sq}i}}{L_i} + \frac{u_{\mathrm{d}i}}{L_i} \\ \dot{I}_{\mathrm{q}i} = -\frac{R_i}{L_i} I_{\mathrm{q}i} - \omega_i I_{\mathrm{d}i} + \frac{V_{\mathrm{sd}i}}{L_i} + \frac{u_{\mathrm{q}i}}{L_i} \end{cases} \tag{1}$$

where $I_{\mathrm{d}i}$ and $I_{\mathrm{q}i}$ are the $i$th $d$-axis and $q$-axis AC current; $V_{\mathrm{sd}i}$ and $V_{\mathrm{sq}i}$ are the $i$th $d$-axis and $q$-axis AC voltage, in the synchronous frame $V_{\mathrm{sd}i} = 0$ and $V_{\mathrm{sq}i} = V_{\mathrm{s}}$; $u_{\mathrm{d}i}$ and $u_{\mathrm{q}i}$ are the $i$th d-axis and q-axis control input of VSC; $R_i$ and $L_i$ are the $i$th resistance and inductance of the VSC transformer and phase reactor. Note that Eq. (1) is actually extended from the two-terminal VSC-HVDC system model [10],

which control inputs are an aggregated term of the difference between the generator side voltage $u_{\mathrm{sq1}}/u_{\mathrm{sd1}}$ and VSC side voltage $u_{\mathrm{rq1}}/u_{\mathrm{rd1}}$. However such forms are not proper to represent the more 'real' control inputs as there are no such control inputs forms in practice, which cannot be applied to the VSC-MTDC systems directly until some algebraic calculations being done. This paper redefines the control inputs with only VSC side voltages $u_{\mathrm{rq1}}/u_{\mathrm{rd1}}$ and they are the 'real' control inputs which can be implemented in VSC-MTDC systems directly, such that the physical meaning of control inputs can be retained.

By neglecting the resistance of the VSC reactor and switching losses, the instantaneous active power $P_i$ and reactive power $Q_i$ on the $i$th AC side of the VSC can be calculated as follows [18]

$$\begin{cases} P_i = \frac{3}{2}(V_{\mathrm{sq}i}I_{\mathrm{q}i} + V_{\mathrm{sd}i}I_{\mathrm{d}i}) = \frac{3}{2}V_{\mathrm{sq}i}I_{\mathrm{q}i} \\ Q_i = \frac{3}{2}(V_{\mathrm{sq}i}I_{\mathrm{d}i} - V_{\mathrm{sd}i}I_{\mathrm{q}i}) = \frac{3}{2}V_{\mathrm{sq}i}I_{\mathrm{d}i} \end{cases} \tag{2}$$

The DC cable dynamics can be expressed by [18]

$$\begin{cases} \dot{V}_{\mathrm{dc}i} = \frac{1}{V_{\mathrm{dc}i}C_i}P_i - \frac{1}{C_i}I_{\mathrm{c}i} \\ \dot{I}_{\mathrm{c}i} = \frac{1}{L_{\mathrm{c}i}}V_{\mathrm{dc}i} - \frac{R_{\mathrm{c}i}}{L_{\mathrm{c}i}}I_{\mathrm{c}i} - \frac{1}{L_{\mathrm{c}i}}V_{\mathrm{cc}} \end{cases} \tag{3}$$

where $C_i$ and $C_{\mathrm{c}}$ are the $i$th and common DC capacitance which voltages are denoted

by $V_{\mathrm{dc}i}$ and $V_{\mathrm{cc}}$, respectively, which locations are given in Fig. 1; $R_{\mathrm{c}i}$ and $L_{\mathrm{c}i}$ are the resistance and inductance of the $i$th DC cable; $I_{\mathrm{c}i}$ is the current through the $i$th DC cable. This paper adopts the same DC cable model as employed in references [10, 15, 16], it considers the DC transmission line to be a long overhead line, in which a $\pi$-link model of the DC circuit is adopted to model the DC cable. Particularly, one leg of $\pi$-link DC cable is connected to each converter while all the other legs of $\pi$-link DC cable of all converters are parallel thus aggregated and represented by the common capacitor $C_{\mathrm{c}}$. This is a reasonable approximation for the purpose of control systems analysis.

The topology of an $N$-terminal VSC-HVDC system is illustrated by Fig. 2 [31], in which $V_{\mathrm{cc}}$ is located at the midpoint to represent a special type of interconnection of $N$ terminals, such that the balance of DC currents of each terminal can be simply described by one differential equation on the common capacitor $C_{\mathrm{c}}$. The dynamics of the common DC capacitor is calculated as

$$\dot{V}_{\mathrm{cc}} = \frac{1}{C_{\mathrm{c}}} \sum_{i=1}^{N} I_{\mathrm{c}i} \tag{4}$$

To this end, the global model of the $N$-terminal VSC-HVDC system is written

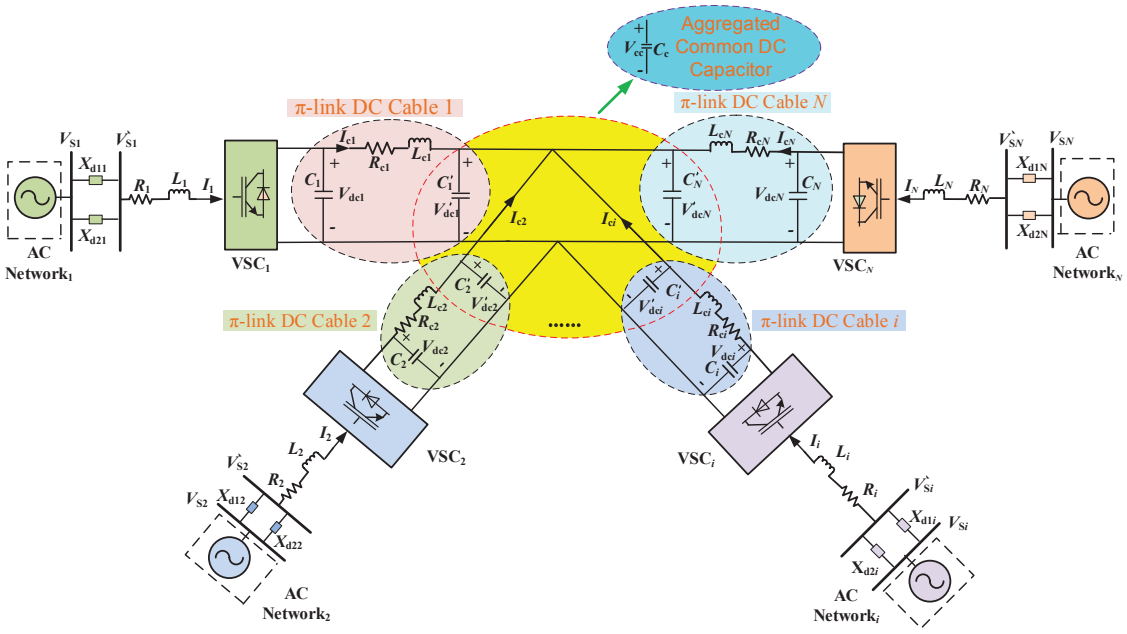


Figure 2: The topology of an $N$-terminal VSC-HVDC system.

as follows

$$\begin{cases} \dot{I}_{\mathrm{d}i} = -\frac{R_i}{L_i} I_{\mathrm{d}i} + \omega_i I_{\mathrm{q}i} + \frac{V_{\mathrm{sq}i}}{L_i} + \frac{u_{\mathrm{d}i}}{L_i} \\ \dot{I}_{\mathrm{q}i} = -\frac{R_i}{L_i} I_{\mathrm{q}i} - \omega_i I_{\mathrm{d}i} + \frac{u_{\mathrm{q}i}}{L_i} \\ \dot{V}_{\mathrm{dc}i} = \frac{3V_{\mathrm{sq}i} I_{\mathrm{q}i}}{2V_{\mathrm{dc}i} C_i} - \frac{1}{C_i} I_{\mathrm{c}i} \qquad , i = 1, \ldots, N \\ \dot{I}_{\mathrm{c}i} = \frac{1}{L_{\mathrm{c}i}} V_{\mathrm{dc}i} - \frac{R_{\mathrm{c}i}}{L_{\mathrm{c}i}} I_{\mathrm{c}i} - \frac{1}{L_{\mathrm{c}i}} V_{\mathrm{cc}} \\ \dot{V}_{\mathrm{cc}} = \frac{1}{C_{\mathrm{c}}} \sum_{i=1}^{N} I_{\mathrm{c}i} \end{cases} \tag{5}$$

The order of system (5) is $4N + 1$. Here, each inverter is equipped with a unique controller to control its active power and reactive power injection in AC networks, while each rectifier is equipped with a unique controller to control its DC voltage and reactive power, respectively.

# 3 Passive Control Design for the $N$-terminal VSC-HVDC System

## 3.1 Passive control

The objective of PC is to passivize the system with a storage function which has a minimum at the desired equilibrium point, hence it reshapes the system energy and assigns a closed-loop energy function equal to the difference between the energy of the system and the energy supplied by the controller. Consider a dynamical nonlinear system represented with the general model

$$\begin{cases} \dot{x} = f(x,u) \\ y = h(x,u) \end{cases} \tag{6}$$

where $x \in R^n$ is the system state vector. $u \in R^m$ and $y \in R^m$ represent the input and output, respectively.

The energy balancing equation can be written as follows:

$$\underbrace{H[x(t)] - H[x(0)]}_{\text{stored}} = \underbrace{\int_0^t u^T(s)y(s)ds}_{\text{supplied}} - \underbrace{d(t)}_{\text{dissipated}} \tag{7}$$

where $H(x)$ is the stored energy function, and $d(t)$ is a nonnegative function that

captures the dissipation effects, e.g., due to resistances or frictions, etc.

System (6) is defined to be output strictly passive if there exists a continuously differentiable positive semi-definite function $H(x)$ (called the storage function) such that

$$u^{\mathrm{T}}y \geq \frac{\partial H}{\partial x} f(x,u) + \zeta y^{\mathrm{T}}y, \quad \forall (x,u) \in R^n \times R^m \tag{8}$$

where $\zeta > 0$. In order to obtain the asymptotic stability the following lemma is needed.

*Lemma.1. Consider the system described in (6), The origin of the uncontrolled system* $\dot{x} = f(x,0)$ *is asymptotically stable if the system is output strictly passive and zero-state detectable with a positive definite storage function* $H(x)$*. Moreover, if the storage function* $H(x)$ *is radially unbounded then the origin is globally asymptotic stable* [21].

If system (6) is not passive, but there exists a positive definite storage function $H(x)$ and a feedback control law $u = \beta(x) + \kappa v$ such that $\dot{H} \leq vy$, then the feedback system is passive. As a result, the feedback passivation can be used as a preliminary

step in a stabilization design because of the additional output feedback

$$v = -\phi(y) \tag{9}$$

where $\phi(y)$ is a sector-nonlinearity satisfying $y\phi(y) > 0$ for $y \neq 0$ and $\phi(0) = 0$, can achieve $\dot{H} \leq -y\phi(y) \leq 0$.

## 3.2 Passive Control Design for Rectifier

For system (5), denote the $j$th VSC as the master controller such that DC voltage $V_{\mathrm{dc}j}$ and reactive power $Q_j$ can be regulated to their reference values $V^*_{\mathrm{dc}j}$ and $Q^*_j$, respectively. Define the tracking error $e_j = [e_{j1}, e_{j2}]^{\mathrm{T}} = [V_{\mathrm{dc}j} - V^*_{\mathrm{dc}j}, Q_j - Q^*_j]^{\mathrm{T}}$, and differentiate $e_j$ until control inputs $u_{\mathrm{q}j}$ and $u_{\mathrm{d}j}$ appear explicitly, gives

$$\begin{cases} \ddot{e}_{j1} = \frac{3V_{\mathrm{sq}j}}{2C_jV_{\mathrm{dc}j}}\Big[-\frac{R_j}{L_j}I_{\mathrm{q}j} + \omega_j I_{\mathrm{d}j} - \frac{I_{\mathrm{q}j}}{C_jV_{\mathrm{dc}j}}\Big(\frac{3V_{\mathrm{sq}j}I_{\mathrm{q}j}}{2V_{\mathrm{dc}j}} - I_{\mathrm{c}j}\Big)\Big] - \frac{1}{C_jL_{\mathrm{c}j}}(V_{\mathrm{dc}j} - R_{\mathrm{c}j}I_{\mathrm{c}j} - V_{\mathrm{cc}}) \\ \qquad + \frac{3V_{\mathrm{sq}j}}{2C_jL_jV_{\mathrm{dc}j}}u_{\mathrm{q}j} - \ddot{V}^*_{\mathrm{dc}j} \\ \dot{e}_{j2} = \frac{3V_{\mathrm{sq}j}}{2}\left(-\frac{R_j}{L_j}I_{\mathrm{d}j} + \omega_j I_{\mathrm{q}j} + \frac{V_{\mathrm{sq}j}}{L_j}\right) + \frac{3V_{\mathrm{sq}j}}{2L_j}u_{\mathrm{d}j} - \dot{Q}^*_j \end{cases} \tag{10}$$

Construct a storage function [23] of system (10) as follows

$$H_j(V_{\mathrm{dc}j}, I_{\mathrm{dc}j}, Q_j) = \frac{1}{2}(V_{\mathrm{dc}j} - V^*_{\mathrm{dc}j})^2 + \frac{1}{2C_j^2}(I_{\mathrm{dc}j} - I^*_{\mathrm{dc}j})^2 + \frac{1}{2}(Q_j - Q^*_j)^2 \tag{11}$$

where $I_{\mathrm{dc}j}$ and $I^*_{\mathrm{dc}j}$ are the current through capacitor $C_j$ and its reference value, respectively, with $I^*_{\mathrm{dc}j} = C_j \frac{\mathrm{d}\, V_{\mathrm{dc}j}}{\mathrm{d}t}|_{V_{\mathrm{dc}j}=V^*_{\mathrm{dc}j}}$.

$H_j$ includes the quadratic sum of the voltage and current of the $j$th DC capacitor and the reactive power in the $j$th AC network. Differentiating $H_j$ with respect to the time, it yields

$$\begin{aligned}
\dot{H}_j &= \frac{1}{C_j}(V_{\mathrm{dc}j} - V^*_{\mathrm{dc}j})(I_{\mathrm{dc}j} - I^*_{\mathrm{dc}j}) + \frac{1}{C_j}(I_{\mathrm{dc}j} - I^*_{\mathrm{dc}j})(\ddot{V}_{\mathrm{dc}j} - \ddot{V}^*_{\mathrm{dc}j}) + (Q_j - Q^*_j)(\dot{Q}_j - \dot{Q}^*_j) \\
&= \frac{1}{C_j}(I_{\mathrm{dc}j} - I^*_{\mathrm{dc}j})\Big\{(V_{\mathrm{dc}j} - V^*_{\mathrm{dc}j}) + \frac{3V_{\mathrm{sq}j}}{2C_jV_{\mathrm{dc}j}}\Big[ - \frac{R_j}{L_j}I_{\mathrm{q}j} + \omega_j I_{\mathrm{d}j} - \frac{I_{\mathrm{q}j}}{C_jV_{\mathrm{dc}j}}\Big(\frac{3V_{\mathrm{sq}j}I_{\mathrm{q}j}}{2V_{\mathrm{dc}j}} - I_{\mathrm{c}j}\Big)\Big] \\
&- \frac{1}{C_jL_{\mathrm{c}j}}(V_{\mathrm{dc}j} - R_{\mathrm{c}j}I_{\mathrm{c}j} - V_{\mathrm{cc}}) + \frac{3V_{\mathrm{sq}j}}{2C_jL_jV_{\mathrm{dc}j}}u_{\mathrm{q}j} - \ddot{V}^*_{\mathrm{dc}j}\Big\} \\
&+ (Q_j - Q^*_j)\Big[\frac{3V_{\mathrm{sq}j}}{2}\left(-\frac{R_j}{L_j}I_{\mathrm{d}j} + \omega_j I_{\mathrm{q}j} + \frac{V_{\mathrm{sq}j}}{L_j}\right) + \frac{3V_{\mathrm{sq}j}}{2L_j}u_{\mathrm{d}j} - \dot{Q}^*_j\Big]
\end{aligned} \tag{12}$$

Design the passive controller for system (10) as

$$\begin{cases}
u_{\mathrm{q}j} = \frac{2C_jL_jV_{\mathrm{dc}j}}{3V_{\mathrm{sq}j}}\Big\{ - (V_{\mathrm{dc}j} - V^*_{\mathrm{dc}j}) + \frac{1}{C_jV_{\mathrm{dc}j}}\Big[\frac{R_j}{L_j}P_j - \omega_jQ_j + \frac{P_j}{C_jV_{\mathrm{dc}j}}\Big(\frac{P_j}{V_{\mathrm{dc}j}} - I_{\mathrm{c}j}\Big)\Big] \\
\qquad + \frac{1}{C_jL_{\mathrm{c}j}}(V_{\mathrm{dc}j} - R_{\mathrm{c}j}I_{\mathrm{c}j} - V_{\mathrm{cc}}) + \ddot{V}^*_{\mathrm{dc}j} + \nu_{j1}\Big\} \\
u_{\mathrm{d}j} = \frac{2L_j}{3V_{\mathrm{sq}j}}\Big[ - \omega_jP_j - \frac{3V^2_{\mathrm{sq}j}}{2L_j} + \frac{R_j}{L_j}Q^*_j + \dot{Q}^*_j + \nu_{j2}\Big]
\end{cases} \tag{13}$$

where $V_j = [\nu_{j1}, \nu_{j2}]^{\mathrm{T}}$ is the additional system input.

Choose the system output for system (10) as $Y_j = [Y_{j1}, Y_{j2}]^{\mathrm{T}} = [(I_{\mathrm{dc}j} - I^*_{\mathrm{dc}j})/C_j, Q_j -$

$Q_j^*]^{\mathrm{T}}$. Let $V_j = [-\lambda_{j1}Y_{j1}, -\lambda_{j2}Y_{j2}]^{\mathrm{T}}$, where $\lambda_{j1}$ and $\lambda_{j2}$ are some positive constants for the feedback passivation to inject an extra damping in $I_{\mathrm{dc}j}$ and $Q_j$. Substituting control (13) into (12) and using (2), it obtains

$$\begin{aligned}\dot{H}_j &= \frac{1}{C_j}(I_{\mathrm{dc}j} - I_{\mathrm{dc}j}^*)\nu_{j1} + (Q_j - Q_j^*)\Big( - \frac{R_j}{L_j}(Q_j - Q_j^*) + \nu_{j2}\Big) \\ &= \nu_{j1}Y_{j1} + \nu_{j2}Y_{j2} - \frac{R_j}{L_j}Y_{j2}^2 \\ &= -\lambda_{j1}Y_{j1}^2 - (\lambda_{j2} + \frac{R_j}{L_j})Y_{j2}^2 \leq 0 \end{aligned} \tag{14}$$

It can be easily verified that the uncontrolled system is zero-state detectable. According to the passivity theory [34], system (10) is output strictly passive from output $Y_j$ to input $V_j$. From power-current relationship (2) and DC dynamics (3), one can conclude that $I_{\mathrm{d}j}$, $I_{\mathrm{q}j}$, and $V_{\mathrm{dc}j}$ are asymptotically stabilized to their reference values $I_{\mathrm{d}j}^*$, $I_{\mathrm{q}j}^*$, and $V_{\mathrm{dc}j}^*$. Note that the regulation of one DC voltage to its set-point may sometimes result in other voltages in the DC networks go to different equilibriums, instead of always go to their respective set-points. In such cases, more converters have to be employed as the rectifiers to ensure the DC networks voltage could be regulated to their respective set-points.

In order to investigate the effect of feedback passivation gains $\lambda_{j1}$ and $\lambda_{j2}$ on the

rectifier controller performance, substitute control (13) into the error dynamics (10). One can obtain the closed-loop system as follows:

$$\begin{cases} \ddot{e}_{j1} + \lambda_{j1}\dot{e}_{j1} + e_{j1} = 0 \\ \dot{e}_{j2} + (\lambda_{j2} + \frac{R_j}{L_j})e_{j2} = 0 \end{cases} \tag{15}$$

From the closed-loop system of rectifier (15), it can be found that its poles are located at $-\frac{\lambda_{j1}}{2} \pm \frac{\sqrt{\lambda_{j1}^2-4}}{2}$ and $-(\lambda_{j2} + \frac{R_j}{L_j})$ for DC voltage and reactive power, respectively. Thus a larger $\lambda_{j1}$ and $\lambda_{j2}$ will result in a faster error convergence. Moreover, one can obtain the transfer function of the closed-loop system of rectifier (15) as

$$\begin{cases} \Phi_{j1}(s) = \frac{1}{\frac{s}{\lambda_{j1}} + \frac{1}{\lambda_{j1}s} + 1} \\ \Phi_{j2}(s) = \frac{1}{\frac{s}{\lambda_{j2}} + \frac{R_j}{L_j\lambda_{j2}} + 1} \end{cases} \tag{16}$$

Hence, the controller bandwidth can be directly calculated as

$$\begin{cases} |\Phi_{j1}(j\omega_{\mathrm{b}j1})| = \frac{1}{\sqrt{2}} \Rightarrow 1 + (\frac{\omega_{\mathrm{b}j1}}{\lambda_{j1}} - \frac{1}{\omega_{\mathrm{b}j1}})^2 = 2 \Rightarrow \omega_{\mathrm{b}j1} = \frac{(\sqrt{5}+1)}{2}\lambda_{j1} \\ |\Phi_{j2}(j\omega_{\mathrm{b}j2})| = \frac{1}{\sqrt{2}} \Rightarrow (\frac{\omega_{\mathrm{b}j2}}{\lambda_{j2}})^2 + (1 + \frac{R_j}{L_j}\lambda_{j2})^2 = 2 \Rightarrow \omega_{\mathrm{b}j2} = \sqrt{\lambda_{j2}^2 - \frac{2R_j}{L_j\lambda_{j2}} - \frac{R_j^2}{L_j^2}} \end{cases} \tag{17}$$

It is worth mentioning that the measurement of $V_{\mathrm{dc}j}$ cannot be accurate due to the sensor noise or external disturbance, which may result in a chattering for the DC

voltage control. In order to handle this issue, a low-pass filter can be used to filter out such chattering. This paper considers only one converter to control DC voltage for the illustration of PC design, it can be easily extended to multiple converters case by denoting them as $j_1, \cdots, j_n$ and design these controllers according to (13), while other converters are then used for active and reactive power control with $k = 1, \cdots, N$, $k \neq j_1, \cdots, j_n$.

## 3.3 Passive Control Design for Inverter

The $k$th VSC is then designed to regulate active power $P_k$ and reactive power $Q_k$ to their reference values $P_k^*$ and $Q_k^*$, respectively, where $k = 1, \cdots, N$ and $k \neq j$. Define tracking error $e_k = [e_{k1}, e_{k2}]^{\mathrm{T}} = [P_k - P_k^*, Q_k - Q_k^*]^{\mathrm{T}}$, and differentiate $e_k$ until control inputs $u_{\mathrm{q}k}$ and $u_{\mathrm{d}k}$ appear explicitly, gives

$$\begin{cases} \dot{e}_{k1} = \frac{3V_{\mathrm{sq}k}}{2}\left(-\frac{R_k}{L_k}I_{\mathrm{q}k} - \omega_k I_{\mathrm{d}k}\right) + \frac{3V_{\mathrm{sq}k}}{2L_k}u_{\mathrm{q}k} - \dot{P}_k^* \\ \dot{e}_{k2} = \frac{3V_{\mathrm{sq}k}}{2}\left(-\frac{R_k}{L_k}I_{\mathrm{d}k} + \omega_k I_{\mathrm{q}k} + \frac{V_{\mathrm{sq}k}}{L_k}\right) + \frac{3V_{\mathrm{sq}k}}{2L_k}u_{\mathrm{d}k} - \dot{Q}_k^* \end{cases} \tag{18}$$

Construct a storage function of system (18) as follows

$$H_k(P_k, Q_k) = \frac{1}{2}(P_k - P_k^*)^2 + \frac{1}{2}(Q_k - Q_k^*)^2 \tag{19}$$

$H_k$ includes the quadratic sum of the active power and reactive power in the $k$th AC network. Differentiating $H_k$ with respect to the time, it yields

$$\begin{aligned}\dot{H}_k &= (P_k - P_k^*)(\dot{P}_k - \dot{P}_k^*) + (Q_k - Q_k^*)(\dot{Q}_k - \dot{Q}_k^*) \\ &= (P_k - P_k^*)\Big[\frac{3V_{\mathrm{sq}k}}{2}\left(-\frac{R_k}{L_k}I_{\mathrm{q}k} - \omega_k I_{\mathrm{d}k}\right) + \frac{3V_{\mathrm{sq}k}}{2L_k}u_{\mathrm{q}k} - \dot{P}_k^*\Big] \\ &+ (Q_k - Q_k^*)\Big[\frac{3V_{\mathrm{sq}k}}{2}\left(-\frac{R_k}{L_k}I_{\mathrm{d}k} + \omega_k I_{\mathrm{q}k} + \frac{V_{\mathrm{sq}k}}{L_k}\right) + \frac{3V_{\mathrm{sq}k}}{2L_k}u_{\mathrm{d}k} - \dot{Q}_k^*\Big] \end{aligned} \tag{20}$$

Design the passive controller for system (18) as

$$\begin{cases} u_{\mathrm{q}k} = \frac{2L_k}{3V_{\mathrm{sq}k}}\left(\omega_k Q_k + \frac{R_k}{L_k}P_k^* + \dot{P}_k^* + \nu_{k1}\right) \\ u_{\mathrm{d}k} = \frac{2L_k}{3V_{\mathrm{sq}k}}\left(-\omega_k P_k - \frac{3V_{\mathrm{sq}k}^2}{2L_k} + \frac{R_k}{L_k}Q_k^* + \dot{Q}_k^* + \nu_{k2}\right) \end{cases} \tag{21}$$

where $V_k = [\nu_{k1}, \nu_{k2}]^{\mathrm{T}}$ is the additional system input.

Choose the system output for system (18) as $Y_k = [Y_{k1}, Y_{k2}]^{\mathrm{T}} = [P_k - P_k^*, Q_k - Q_k^*]^{\mathrm{T}}$. Let $V_k = [-\lambda_{k1}Y_{k1}, -\lambda_{k2}Y_{k2}]^{\mathrm{T}}$, where $\lambda_{k1}$ and $\lambda_{k2}$ are some positive constants for the feedback passivation to inject an extra damping in $P_k$ and $Q_k$. Substituting control (21) into (20) and using (2), it yields

$$\begin{aligned}\dot{H}_k &= (P_k - P_k^*)\left(-\frac{R_k}{L_k}(P_k - P_k^*) + \nu_{k1}\right) + (Q_k - Q_k^*)\left(-\frac{R_k}{L_k}(Q_k - Q_k^*) + \nu_{k2}\right) \\ &= \nu_{k1}Y_{k1} + \nu_{k2}Y_{k2} - \frac{R_k}{L_k}Y_{k1}^2 - \frac{R_k}{L_k}Y_{k2}^2 \\ &= -(\lambda_{k1} + \frac{R_k}{L_k})Y_{k1}^2 - (\lambda_{k2} + \frac{R_k}{L_k})Y_{k2}^2 \leq 0 \end{aligned} \tag{22}$$

Similarly, system (18) is output strictly passive from output $Y_k$ to input $V_k$. Thus $I_{\mathrm{d}k}$, $I_{\mathrm{q}k}$, and $V_{\mathrm{dc}k}$ are asymptotically stabilized to their reference values $I_{\mathrm{d}k}^*$, $I_{\mathrm{q}k}^*$, and $V_{\mathrm{dc}k}^*$.

In order to further investigate the effect of feedback passivation gains $\lambda_{k1}$ and $\lambda_{k2}$ on the inverter controller performance, substitute control (21) into the error dynamics (18). One can obtain the closed-loop system as follows:

$$\begin{cases} \dot{e}_{k1} + (\lambda_{k1} + \frac{R_k}{L_k})e_{k1} = 0 \\ \dot{e}_{k2} + (\lambda_{k2} + \frac{R_k}{L_k})e_{k2} = 0 \end{cases} \tag{23}$$

From the closed-loop system of inverters (23), it can be found that its poles are located at $-(\lambda_{k1}+\frac{R_k}{L_k})$ and $-(\lambda_{k2}+\frac{R_k}{L_k})$ for active power and reactive power, respectively. Thus a larger $\lambda_{k1}$ and $\lambda_{k2}$ will result in a faster error convergence. Furthermore, one

can obtain the transfer function of the closed-loop system of inverter (23) as

$$\begin{cases} \Phi_{k1}(s) = \frac{1}{\frac{s}{\lambda_{k1}} + \frac{R_k}{L_k \lambda_{k1}} + 1} \\ \Phi_{k2}(s) = \frac{1}{\frac{s}{\lambda_{k2}} + \frac{R_k}{L_k \lambda_{k2}} + 1} \end{cases} \tag{24}$$

Hence, the controller bandwidth can be directly calculated as

$$\begin{cases} |\Phi_{k1}(j\omega_{\mathrm{b}k1})| = \frac{1}{\sqrt{2}} \Rightarrow (\frac{\omega_{\mathrm{b}k1}}{\lambda_{k1}})^2 + (1 + \frac{R_k}{L_k}\lambda_{k1})^2 = 2 \Rightarrow \omega_{\mathrm{b}k1} = \sqrt{\lambda_{k1}^2 - \frac{2R_k}{L_k \lambda_{k1}} - \frac{R_k^2}{L_k^2}} \\ |\Phi_{k2}(j\omega_{\mathrm{b}k2})| = \frac{1}{\sqrt{2}} \Rightarrow (\frac{\omega_{\mathrm{b}k2}}{\lambda_{k2}})^2 + (1 + \frac{R_k}{L_k}\lambda_{k2})^2 = 2 \Rightarrow \omega_{\mathrm{b}k2} = \sqrt{\lambda_{k2}^2 - \frac{2R_k}{L_k \lambda_{k2}} - \frac{R_k^2}{L_k^2}} \end{cases} \tag{25}$$

The roots of the overall closed-loop system are illustrated by Fig. 3. It can be readily observed that a faster error convergence can be achieved as feedback passivation gains $\lambda_{j1}$, $\lambda_{j2}$, $\lambda_{k1}$, and $\lambda_{k2}$ increase. In particular, when $2 \geq \lambda_{j1} > 0$, an exponentially oscillatory convergence of DC voltage will be resulted in; when $\lambda_{j1} \geq 2$, an exponentially monotonic convergence of DC voltage will be obtained.

To this end, inequalities (14) and (22) indicate that systems (10) and (18) can be asymptotically stabilized to the desired equilibrium point as the energy fluctuations converge to zero. The overall storage function $H_{\mathrm{t}}$ of the $N$-terminal VSC-HVDC

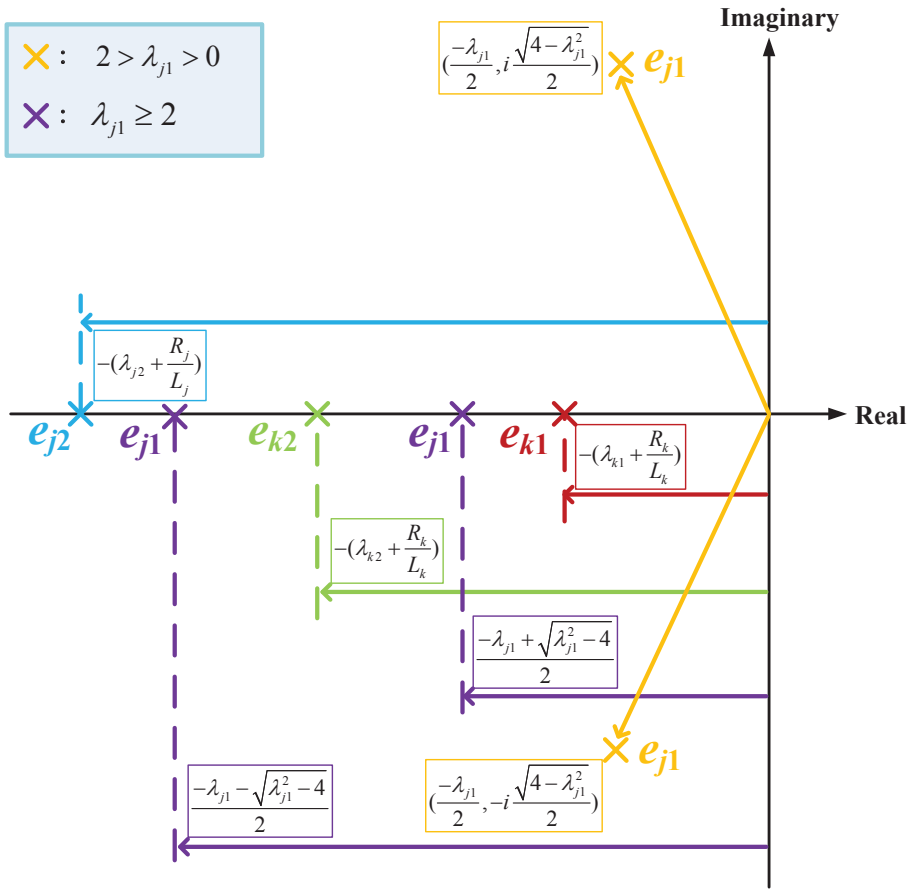


Figure 3: Closed-loop system roots distributions of the rectifiers and inverters of PC.

system (5) by controls (13) and (21) can be expressed in the following form

$$H_{\mathrm{t}} = H_j(V_{\mathrm{dc}j}, I_{\mathrm{dc}j}, Q_j) + \sum_{k=1,k\neq j}^{N} H_k(P_k, Q_k) \tag{26}$$

The structure of the proposed PC design can be illustrated by the block diagram in Fig. 4.

**Remark.1** The conventional linear PI/PID control scheme employs an inner current loop to regulate the current [9], which could employs a synchronous reference frame (SRF) based current controller [33] to avoid overcurrent. In contrast, the proposed nonlinear PC (13) and (21) actually contains no current in its control law while it cannot handle the overcurrent. Hence, the overcurrent protection devices [37–39] will be activated to prevent the overcurrent to grow, which can be seen in Fig. 4.

## 3.4 Internal Dynamics Stability

Under controls (13) and (21), the total system order of active power $P_i$, reactive power $Q_i$, and DC cable voltage $V_{\mathrm{dc}i}$ can be calculated as $N + N + N = 3N$, which can all be asymptotically stabilized. The internal dynamics is related to the DC cable current $I_{\mathrm{c}i}$ and common DC voltage $V_{\mathrm{cc}}$. To simplify the analysis, shift the reference values of the overall system to the origin and the following new state variable vector

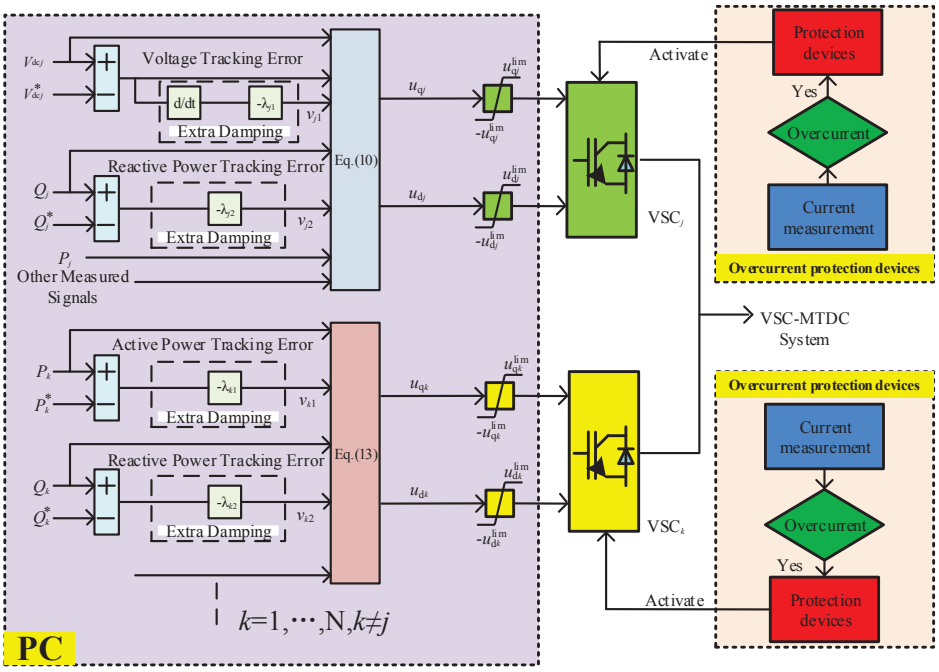


Figure 4: Block diagram of the passive controller.

is introduced as $x = [\tilde{I}_{\mathrm{d}i}, \tilde{I}_{\mathrm{q}i}, \tilde{V}_{\mathrm{dc}i}, \tilde{I}_{\mathrm{c}i}, \tilde{V}_{\mathrm{cc}}]^{\mathrm{T}}$. where $\tilde{x}_i = x_i - x_i^*$ is denoted as the estimation errors of $x_i$ and $x_i^*$ is its reference value, respectively.

System (5) can be expressed in terms of the new state variables as

$$\begin{cases} \dot{\tilde{I}}_{\mathrm{d}i} = -\frac{R_i}{L_i}\tilde{I}_{\mathrm{d}i} + \omega_i \tilde{I}_{\mathrm{q}i} + \frac{\tilde{u}_{\mathrm{d}i}}{L_i} \\ \dot{\tilde{I}}_{\mathrm{q}i} = -\frac{R_i}{L_i}\tilde{I}_{\mathrm{q}i} + \omega_i \tilde{I}_{\mathrm{d}i} + \frac{\tilde{u}_{\mathrm{q}i}}{L_i} \\ \dot{\tilde{V}}_{\mathrm{dc}i} = \frac{3V_{\mathrm{sq}i}I_{\mathrm{q}i}}{2V_{\mathrm{dc}i}C_i} - \frac{3V_{\mathrm{sq}i}I^*_{\mathrm{q}i}}{2V^*_{\mathrm{dc}i}C_i} - \frac{1}{C_i}\tilde{I}_{\mathrm{c}i} \ , i = 1, \ldots, N \\ \dot{\tilde{I}}_{\mathrm{c}i} = \frac{1}{L_{\mathrm{c}i}}\tilde{V}_{\mathrm{dc}i} - \frac{R_{\mathrm{c}i}}{L_{\mathrm{c}i}}\tilde{I}_{\mathrm{c}i} - \frac{1}{L_{\mathrm{c}i}}\tilde{V}_{\mathrm{cc}} \\ \dot{\tilde{V}}_{\mathrm{cc}} = \frac{1}{C_{\mathrm{c}}}\sum_{i=1}^{N}\tilde{I}_{\mathrm{c}i} \end{cases} \tag{27}$$

Divide the state variable vector $\tilde{x}$ into two parts as the output $\eta = [\tilde{I}_{\mathrm{d}i}, \tilde{I}_{\mathrm{q}i}, \tilde{V}_{\mathrm{dc}i}]^{\mathrm{T}}$ and internal state $\xi = [\tilde{I}_{\mathrm{c}i}, \tilde{V}_{\mathrm{cc}}]^{\mathrm{T}}$. Now system (27) can be considered as the normal form [34]

$$\begin{cases} \dot{\eta} = f_1(\eta, \xi, u) \\ \dot{\xi} = f_2(\eta, \xi) \end{cases} \tag{28}$$

with

$$u = f_3(\eta, \xi) \tag{29}$$

When output $\eta$ is identically zero, the behaviour of system (28) is governed by the differential equation

$$\dot{\xi} = f_2(0, \xi) \tag{30}$$

which is the zero-dynamics of system (28).

Based on the previous analysis and power-current relationship (2), it has been proved that $\tilde{V}_{\mathrm{dc}i}$, $\tilde{I}_{\mathrm{d}i}$, and $\tilde{I}_{\mathrm{q}i}$ are asymptotically stable by control (13) and (21). It remains now to study the behaviour of internal state $\xi$ when $\eta$ converges to zero. Substitute $\eta = 0$, $\xi$ is governed by the following differential equation

$$[\dot{\tilde{I}}_{\mathrm{c}1}, \dot{\tilde{I}}_{\mathrm{c}2}, \ldots, \dot{\tilde{I}}_{\mathrm{c}N}, \dot{\tilde{V}}_{\mathrm{cc}}]^{\mathrm{T}} = A[\tilde{I}_{\mathrm{c}1}, \tilde{I}_{\mathrm{c}2}, \ldots, \tilde{I}_{\mathrm{c}N}, \tilde{V}_{\mathrm{cc}}]^{\mathrm{T}} \tag{31}$$

where

$$A = \begin{bmatrix} -\frac{R_{\mathrm{c}1}}{L_{\mathrm{c}1}} & 0 & \cdots & 0 & -\frac{1}{L_{\mathrm{c}1}} \\ 0 & -\frac{R_{\mathrm{c}2}}{L_{\mathrm{c}2}} & \cdots & 0 & -\frac{1}{L_{\mathrm{c}2}} \\ \vdots & \vdots & \ddots & \vdots & \vdots \\ 0 & 0 & \cdots & -\frac{R_{\mathrm{c}N}}{L_{\mathrm{c}N}} & -\frac{1}{L_{\mathrm{c}N}} \\ \frac{1}{C_{\mathrm{c}}} & \frac{1}{C_{\mathrm{c}}} & \cdots & \frac{1}{C_{\mathrm{c}}} & 0 \end{bmatrix}_{(N+1)\times(N+1)} \tag{32}$$

Thus, the zero-dynamics of system (27) becomes

$$\dot{\xi} = A\xi \tag{33}$$

To study the stability of zero-dynamics (33), choose a Lyapunov function as

$$V(\tilde{I}_{ci}, \tilde{V}_{\rm cc}) = \sum_{i=1}^{N} \frac{L_{ci}}{2C_{\rm c}} \tilde{I}_{ci}^2 + \frac{1}{2}\tilde{V}_{\rm cc}^2 \tag{34}$$

The derivative of $V$ along the trajectories of (33) is given by

$$\begin{aligned}
\dot{V} &= \sum_{i=1}^{N} \frac{L_{ci}}{C_{\rm c}} \tilde{I}_{ci}\dot{\tilde{I}}_{ci} + \tilde{V}_{\rm cc}\dot{\tilde{V}}_{\rm cc} \\
&= \sum_{i=1}^{N} \frac{L_{ci}}{C_{\rm c}} \tilde{I}_{ci} \left( -\frac{R_{ci}}{L_{ci}} \tilde{I}_{ci} - \frac{1}{L_{ci}} \tilde{V}_{\rm cc} \right) + \frac{\tilde{V}_{\rm cc}}{C_{\rm c}} \sum_{i=1}^{N} \tilde{I}_{ci} \\
&= -\sum_{i=1}^{N} \frac{R_{ci}}{C_{\rm c}} \tilde{I}_{ci}^2 \leq 0
\end{aligned} \tag{35}$$

It is obvious that $\dot{V}$ is negative semi-definite as $R_{ci} > 0$ and $C_{\rm c} > 0$. To find the neighbourhood of origin $\mathcal{S} = [\xi \in \mathbb{R}^{N+1} | \dot{V}(\xi) = 0]$, note that

$$\dot{V}(\xi) = 0 \Rightarrow \tilde{I}_{ci} = 0, i = 1, \ldots, N \tag{36}$$

Thus $\mathcal{S} = [\xi \in \mathbb{R}^{N+1} | \tilde{I}_{ci} = 0, i = 1, \ldots, N]$. Let $\xi$ be a solution that belongs identically to $\mathcal{S}$:

$$\tilde{I}_{ci} \equiv 0 \Rightarrow \dot{\tilde{I}}_{ci} \equiv 0 \Rightarrow \tilde{V}_{\rm cc} \equiv 0 \tag{37}$$

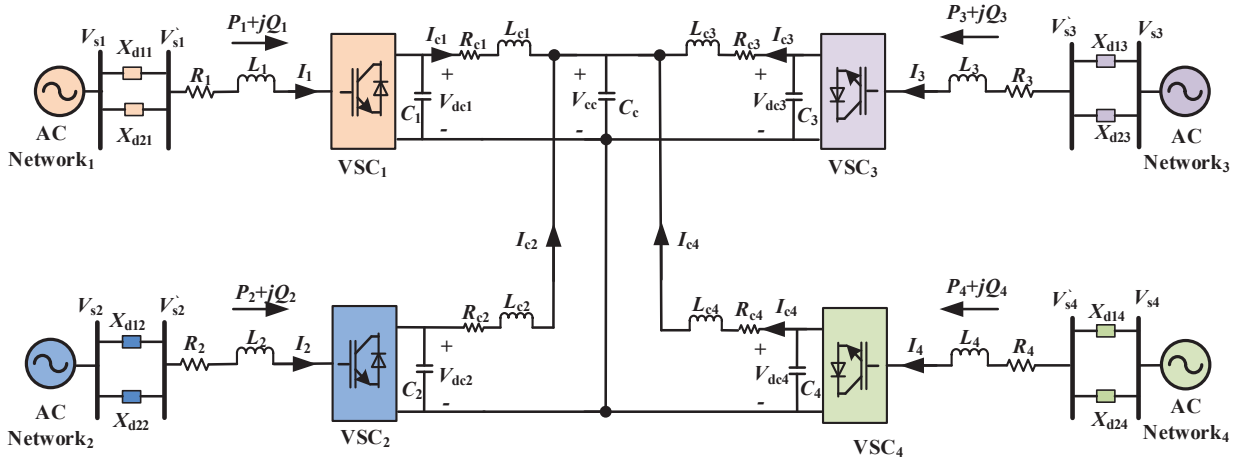


Figure 5: A four-terminal VSC-HVDC system.

Therefore, the only solution that can stay identically in $\mathcal{S}$ is the trivial solution $\xi \equiv 0$. According to LaSalle's theorem and its corollary [34], the zero-dynamics of system (27) is asymptotically stable.

To this end, the whole system (27) can be asymptotically stabilized at $(\eta, \xi) = (0, 0)$ under the proposed controls (13) and (21).

# 4 Simulation Results

The proposed controller is tested in a four-terminal VSC-HVDC system, as illustrated in Fig. 5, which is an extended system from [31]. Note that $\text{VSC}_1$ is chosen as the master controller to regulate the DC voltage and reactive power, while the other three VSCs independently control their active power and reactive power. The system

frequency of AC network$_4$ is 60 Hz, and the others are 50 Hz. All other system parameters are given in Table 1. In addition, four identical three-level neutral-point-clamped VSCs model for each rectifier and inverter from Matlab/Simulink SimPowerSystems are employed, which structure and parameters are taken directly from [9].

The control performance is evaluated under various operation conditions in a wide neighbourhood of the initial operation points and compared to that of PI control [9] and FLC [10, 31]. Here, PI control owns a standard cascade control structure having inner loop current controllers and then outer loop voltage/power controllers, together with the standard decoupling of d-axis and q-axis, while the voltage at the PCC is measured to simplify the inner current loop [9]. Through trial-and-error, PI parameters are chosen as follows: DC voltage loop: $K_{\mathrm{p}} = 80$, $K_{\mathrm{I}} = 120$; Active power/Reactive power loop: $K_{\mathrm{p}} = 6$, $K_{\mathrm{I}} = 10$; d-axis and q-axis current loop: $K_{\mathrm{p}} = 250$, $K_{\mathrm{I}} = 600$. The simulation is executed on Matlab 7.10 using a personal computer with an IntelR Core$^{\mathrm{TM}}$i7 CPU at 2.2 GHz and 4 GB of RAM.

Through trial-and-error, PC parameters are chosen to make a trade-off between the system damping and control costs as follows: For VSC$_1$ rectifier controller: $\lambda_{11} = 250$, $\lambda_{12} = 400$; For VSC$_k$ inverter controller, where $k = 2, 3, 4$; $\lambda_{k1} = \lambda_{k2} = 500$. According to the system parameters from Table 1, the controller bandwidth can be

Table 1: System parameters used in the four-terminal VSC-HVDC system.

| | |
|---|---|
| Base power | $S_{\text{base}}$=100 MVA |
| AC base voltage | $V_{\text{ACbase}}$=100 kV |
| DC base voltage | $V_{\text{DCbase}}$=200 kV |
| AC system resistance (25 km) | $R_i = 0.022\ \Omega$/km |
| AC system inductance (25 km) | $L_i = 2.6$ mH/km |
| DC cable resistance (50 km) | $R_{ci} = 0.016\ \Omega$/km |
| DC cable inductance (50 km) | $L_{ci} = 2.2$ mH/km |
| DC link capacitance | $C_i = 7.96\ \mu$F |
| Common DC capacitance | $C_{\text{c}} = 19.95\ \mu$F |

calculated based on (17) and (25) as: $\omega_{\text{b}11} = 404.5$ rad/s, $\omega_{\text{b}12} = 391.36$ rad/s, and $\omega_{\text{b}k1} = \omega_{\text{b}k2} = 491.39$ rad/s, respectively. The control inputs are bounded as $|u_{\text{q}i}| \leq 1$ p.u., $|u_{\text{d}i}| \leq 1$ p.u., where $i = 1, \ldots, 4$.

*1) Case 1: Active power and reactive power reversal with parameter uncertainties.* An active power and reactive power reversal started at $t = 0.5\ s$ and restored to the original value at $t = 1\ s$ under 20% increase of DC cable resistance has been tested, when the DC voltage is regulated at its nominal value. The system responses are provided by Fig. 6. One can find that the overshoot of active power and reactive power is completely eliminated by PC and FLC compared to that of PI control thanks to the nonlinearities compensation. In addition, PC tracks the reference power more rapidly than that of FLC as it remains the beneficial nonlinearity instead of the exact nonlinearity cancelation, which can also effectively attenuate the malignant effect of DC cable parameter uncertainties against FLC thanks to the improved damping by

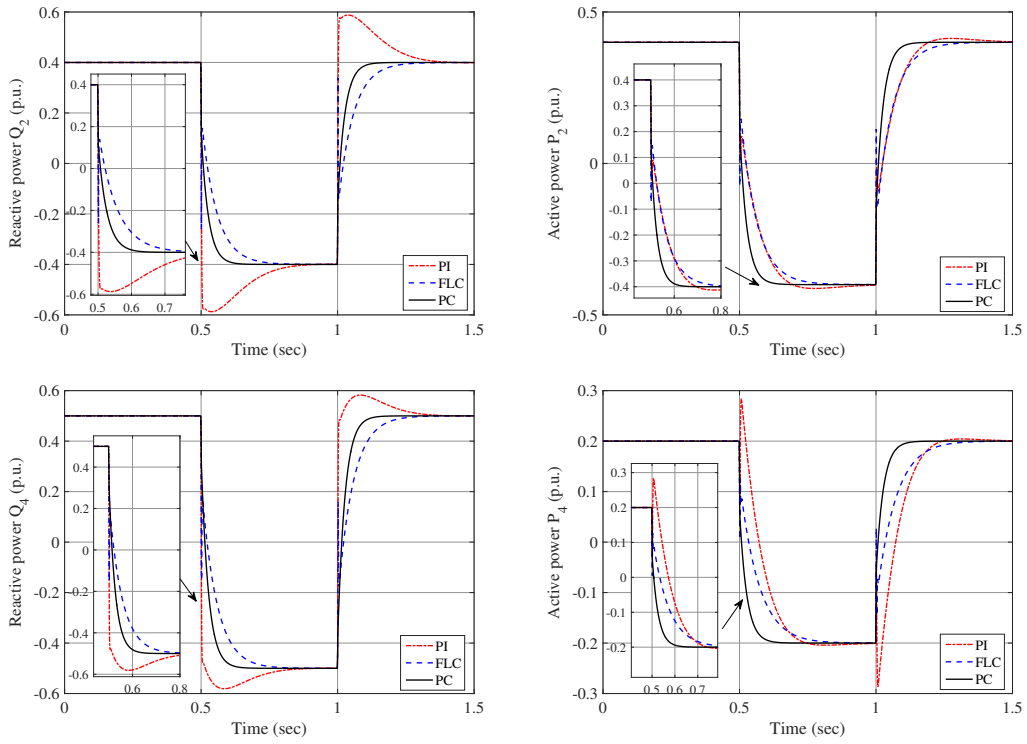


Figure 6: System responses obtained in active power and reactive power reversals under 20% increase of DC cable resistance.

energy shaping. Note that PI control performance is degraded dramatically under varied operation points as its control parameters are tuned based on the one-point linearization.

*2) Case 2: 10-cycle line-line-line-ground (LLLG) fault at AC bus.* A 10-cycle LLLG fault occurs at bus 1 from 0.2 $s$ to 0.4 $s$. Due to the fault, the AC voltage at the corresponding bus is decreased to a critical level [35, 36]. Fig. 7 shows that PC can effectively restore the system with less active power oscillations. Note that

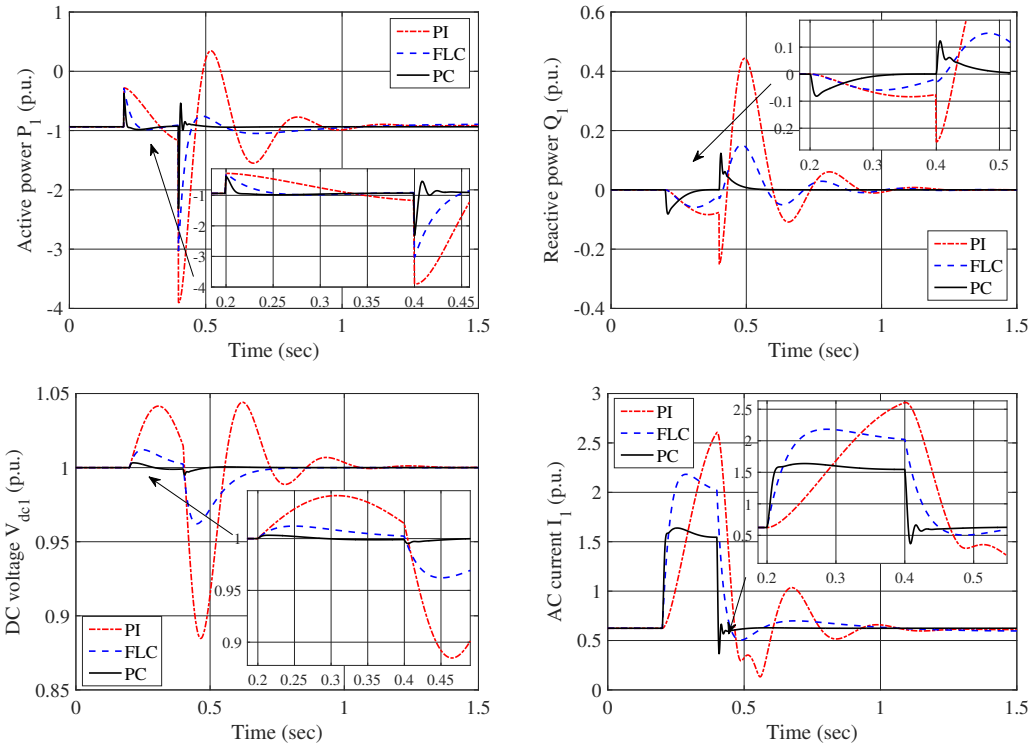


Figure 7: System responses obtained under a 10-cycle LLLG fault at bus 1.

a relatively large overshoot of the AC-side current is resulted in by the PI controller under the AC-side fault, while a smaller current overshoot and a better transient response are provided by the PC and the FLC due to the compensation of the nonlinear dynamics caused by the sudden drop of the AC-side voltage.

*3) Case 3: Temporary fault at the DC cable.* A 5 $ms$ temporary short-circuit fault occurs at the midpoint of DC $\text{cable}_3$ at $t = 1$ $s$ and removed automatically thereafter, which is normally the fastest response time of DC protection system. DC fault will cause a voltage drop in the DC cable and generate a significant transient fault current

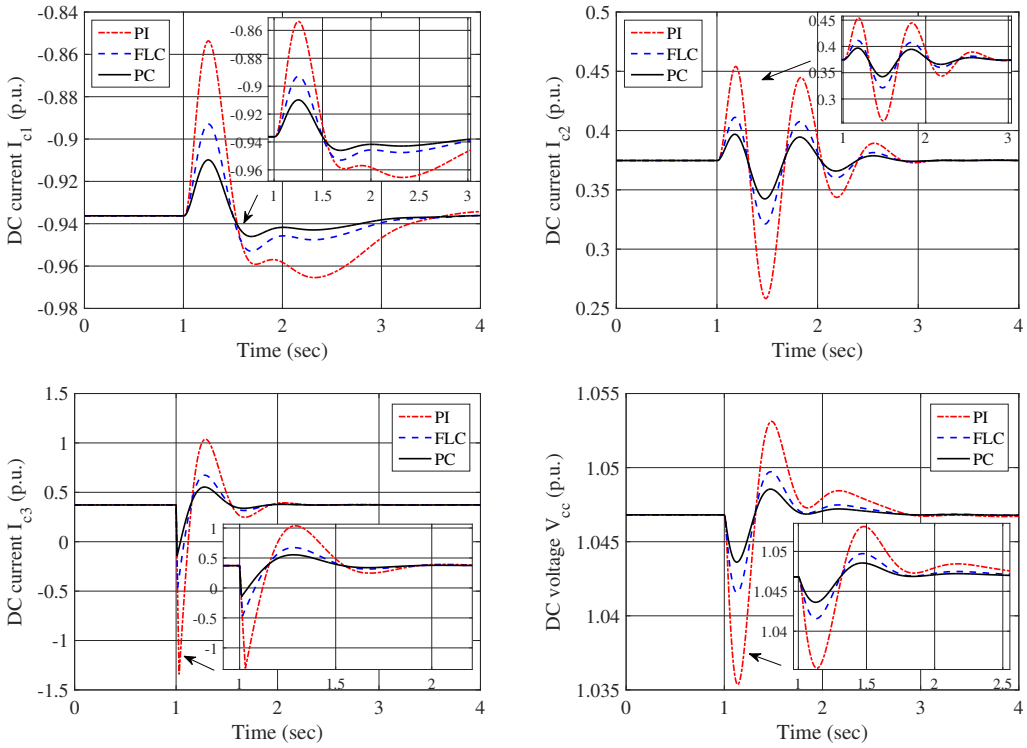


Figure 8: System responses obtained under a 5 *ms* DC fault at the midpoint of DC cable 3.

which may exceed the VSC rated power [40]. Fig. 8 illustrates the corresponding system responses, it can be found that DC currents $I_{c1}$, $I_{c2}$, and $I_{c3}$ can be restored more rapidly and smoothly by PC. Moreover, it can reduce the possibility of VSC overloading when DC fault occurs as less faulty current and common DC voltage $V_{cc}$ produced in comparison to that of FLC and PI control, thus the system stability can be enhanced.

*4) Case 4: Offshore wind farm connection.* When offshore wind farms are con-

nected to the multi-terminal VSC-HVDC system, the terminal voltage $V_{si}$ becomes a time-varying function due to the intermittence nature and stochastic variation of wind energy [41–45]. AC network$_1$ and AC network$_4$ are modelled as two offshore wind farms to investigate the control performance of different approaches, a random 15 $s$ voltage fluctuation mimicking the wind farm output power variation is simulated. System responses are illustrated in Fig. 9, it shows that both active and reactive powers are oscillatory, in which PC has the smallest oscillation magnitude of the control outputs. Hence PC can effectively suppress such power oscillations.

*5) Case 5: Weak AC grid connection.* Consider a weak AC network connection which needs to consider the reactance between AC infinite buses and the PCC. Here, $X_{\mathrm{d1}i}$=$X_{\mathrm{d2}i}$=0.2 p.u. and one of the parallel line in AC network$_1$ and AC network$_3$ are disconnected from the operation at 1 $s$ and again reconnected at 3 $s$ [14]. The obtained system responses are demonstrated by Fig. 10. One can readily see that PC can restore the disturbed system at the fastest rate and the least overshoot in comparison to that of PI control and FLC thanks to its extra system damping injection.

*6) Case 6: Robustness of DC cable resistance uncertainties.* In order to evaluate the robustness against DC cable parameter fluctuations, a series of plant-model mismatches of DC cable resistance $R_{\mathrm{c1}}$ variation around its nominal value due to the

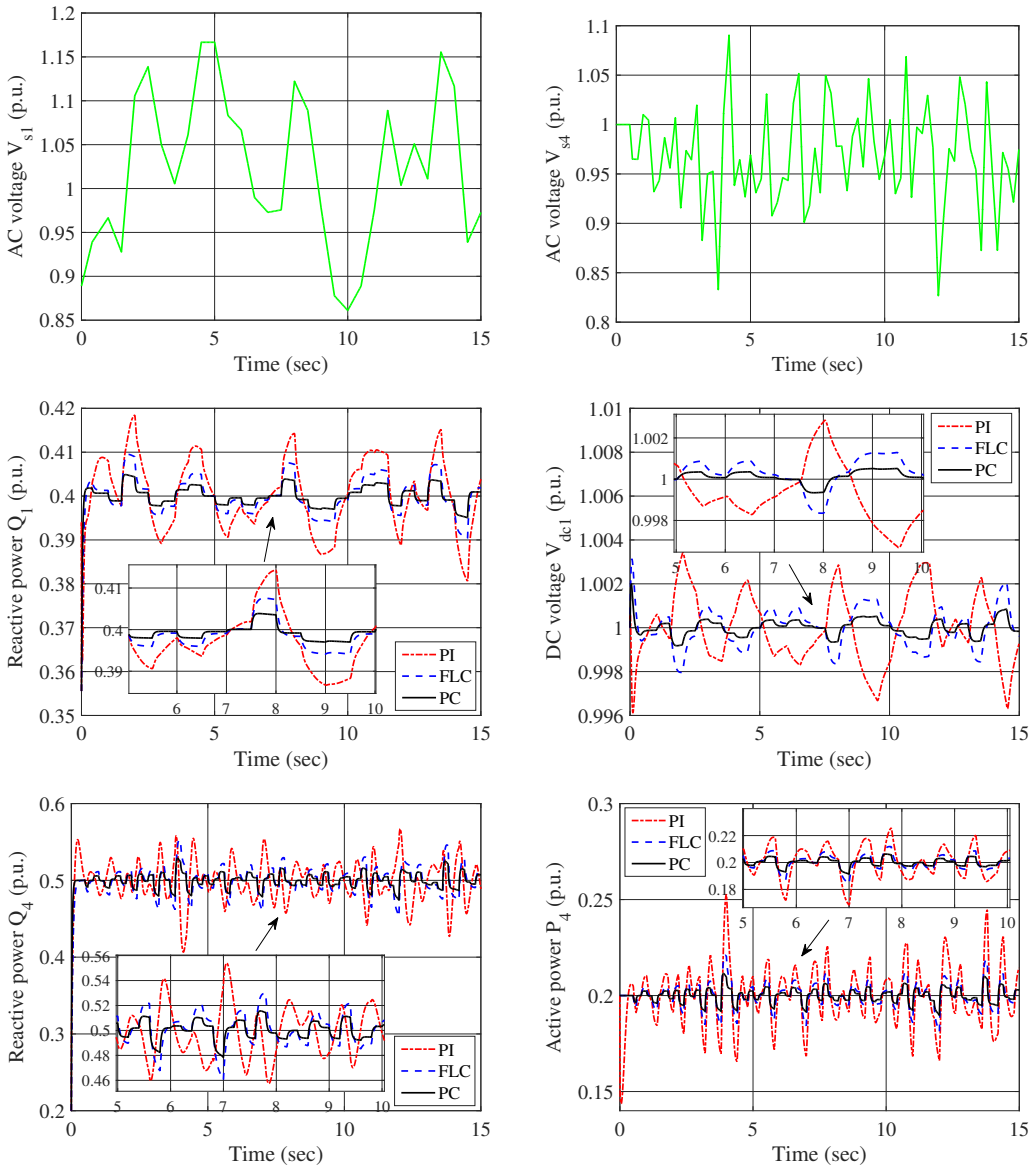


Figure 9: System responses obtained when offshore wind farms are connected.

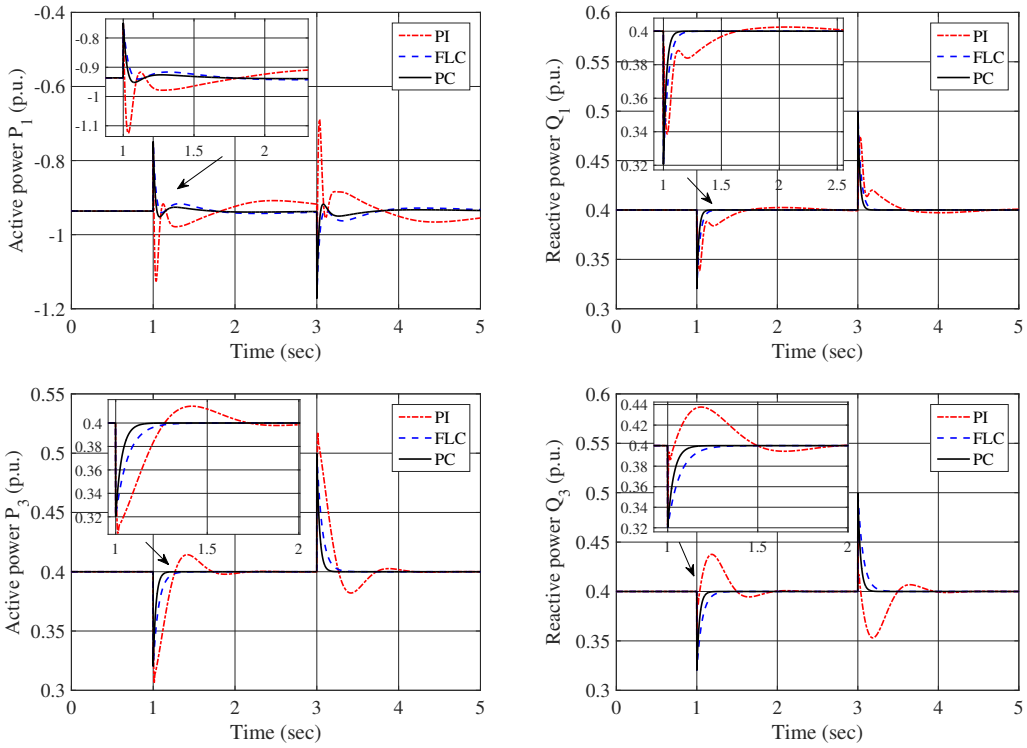


Figure 10: System responses obtained under weak AC network.

temperature variations in the DC cable are undertaken, in which a 5-cycle LLLG fault at bus 1 is applied. The absolute peak value of reactive power $|Q_1|$ and DC voltage $|V_{\mathrm{dc1}}|$ is recorded for a clear comparison. Fig. 11 illustrates that the variation of reactive power $|Q_1|$ obtained by PI control, FLC, and PC is 6.38%, 8.19%, 4.76%, respectively. Meanwhile, the variation of DC voltage $|V_{\mathrm{dc1}}|$ obtained by PI control, FLC, and PC is 5.97%, 7.65%, 4.23%, respectively. It is worth noting that PC can provide the greatest robustness thanks to its additional damping injection mechanism, which can strongly suppress the malignant effect of DC cable parameter fluctuations.

# 5 Discussions

Note that PC design is more complicated than that of PI, which is a quite common issue for these advanced control design [15] according to the "no free lunch theorem". In order to improve the control performance, or enhance robustness/adaptiveness, etc., a sacrifice of control system simplicity is usually unavoidable. Fortunately, thanks to the fast development of modern control system and advanced electronics, more and more advanced controllers are implementable and have been validated by hardware-in-loop test [10–17]. It is therefore promising that PC could be implemented in practice by those state-of-art techniques.

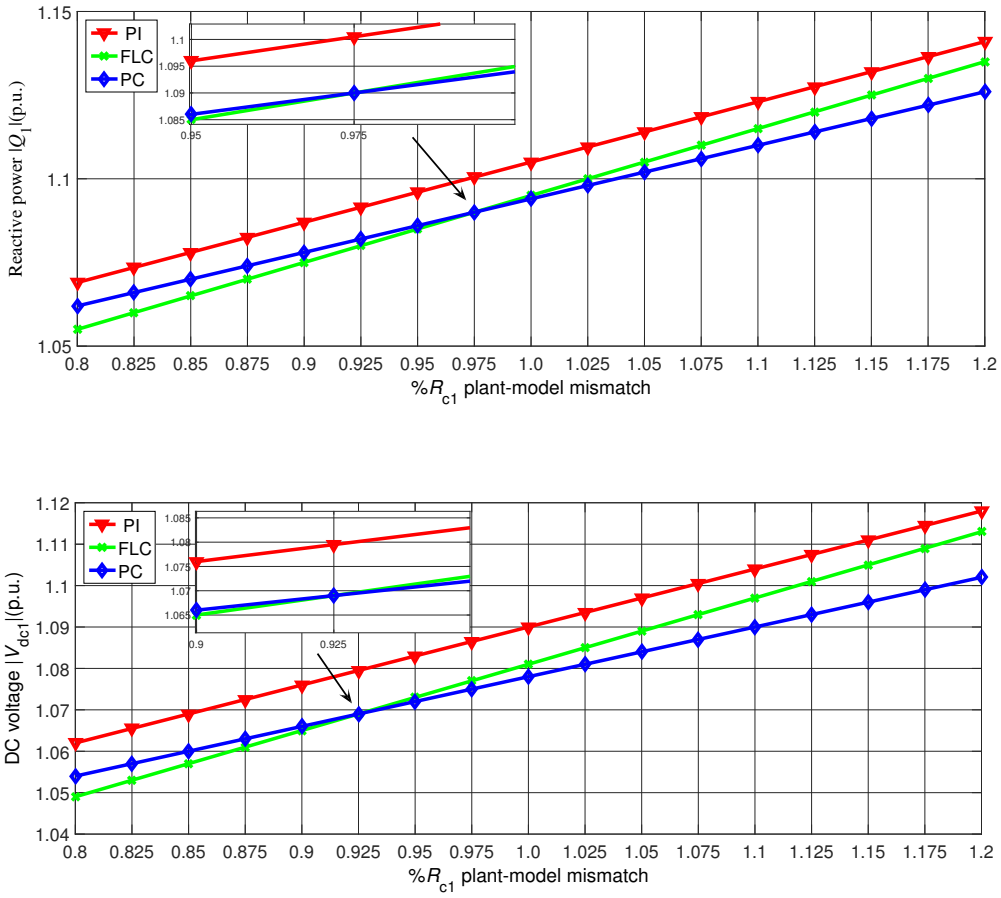


Figure 11: System robustness obtained under the DC cable resistance uncertainties.

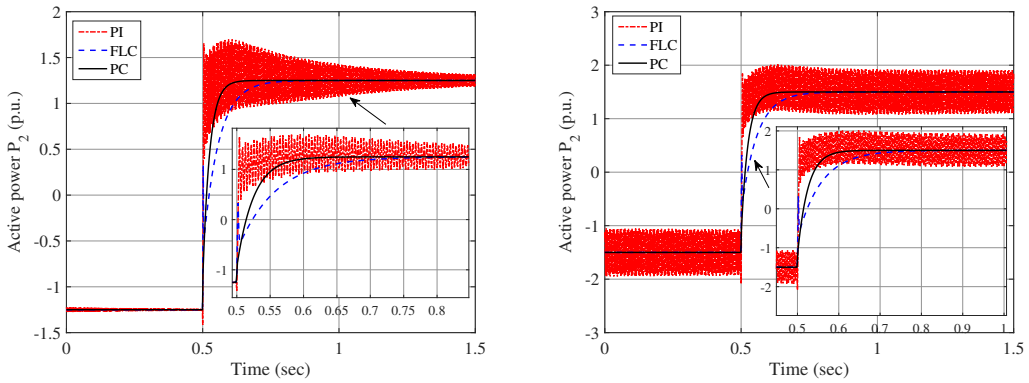


Figure 12: System responses obtained under large power reversal at AC network$_2$.

Moreover, through trial-and error, it has been found that a power reversal started from -1.25 p.u. to 1.25 p.u. of active power of AC network$_2$ will cause a long-lasting oscillation of active power by PI control. In addition, when the power reversal grows even larger, e.g., from -1.5 p.u. to 1.5 p.u., a consistent oscillation will be resulted in. In contrast, PC can still maintain a stable and satisfactory control performance, as shown in Fig. 12. Hence the benefit of PC (global control consistency) can be clearly verified compared to PI (control performance degradation and power oscillation) despite of its complicated control structure.

Lastly, the application of PC to other VSC-HVDC systems are summarized as follows:

• If the VSC-HVDC system is connected to some passive networks without generation, the proposed PC cannot be employed on the inverter side connecting to the

passive networks, which requires to regulate the AC voltage [46] to be a constant. This is because that the relationship between system output and control input is an algebraic equation, which cannot be used to construct a storage function, thus one cannot obtain the PC by differentiating the storage function. However, a hybrid PC and PI control framework can be adopted, e.g., PC is deisgned for rectifier side and inverter side connecting to active networks, while PI control is designed for inverter side connecting to passive networks.

- If the VSC-HVDC system is embedded in AC networks, in which AC areas are also connected by AC tie-lines [47]. The proposed PC can directly be applied to achieve the following three control objectives: (1) active power; (2) reactive power; and (3) DC voltage. As the control input can be explicitly derived by differentiating the storage function consisted of system output, while PC does not require the information of the AC tie-line.

- If the $N$ terminals of VSC-MTDC system are in other configurations, e.g. meshed DC network. In general, there're four ways to regulate the DC power flow [48]: (1) Adjusting DC resistances of transmission lines; (2) Adopting a DC transformer; (3) Inserting an auxiliary voltage source into the transmission line; and (4) Interline power flow controller. However, the relationship between system output and control input of these methods are all in algebraic form, thus the storage function

cannot be constructed and PC cannot be applied into meshed DC network. In fact, most of these controllers have used PID/PI based method for meshed DC networks.

# 6 Conclusion

In this paper, a passive control scheme has been developed for multi-terminal VSC-HVDC system, which can effectively transmit the electrical power from renewable power generations. The storage function is reshaped into an output strictly passive form, in which the beneficial nonlinearities are retained to provide a better transient performance of the active power, reactive power, and direct current cable voltage. Then the closed-loop system stability has been proved to be asymptotically stable by the zero-dynamics technique.

Case studies have been carried out on a four-terminal VSC-HVDC system, a comprehensive comparison has been undertaken with the one-point linearization based PI control and the full nonlinearities cancelation based FLC. The regulation performance of active power and reactive power is tested, together with a typical power reversal, which demonstrates that PC can achieve a rapid power tracking and eliminate the overshoot. Then its control performance is evaluated under faults at AC bus and DC cable, offshore wind farm connections, weak AC grid connection, and robustness of DC cable resistance uncertainties. Simulation results demonstrate that

PC can restore the disturbed system more effectively than others, while the fault current of PC is minimal, thus it can reduce the possibility of VSC overloading.

Future work will be carried out on the following aspects: (1) Converter losses will be considered to develop a more practical system model; (2) Bipolar VSC configuration will be taken into account to study the different system structure; (3) VSC capability curves will be introduced to provide a thorough VSC operation performance; and (4) A hardware-in-loop test (HIL) will be undertaken to test the proposed controller in practical transient stability studies.

## Acknowledgements

The authors gratefully acknowledge the support of National Natural Science Foundation of China (51477055, 51667010, 51777078), Yunnan Provincial Talents Training Program (KKSY201604044), and Scientific Research Foundation of Yunnan Provincial Department of Education (KKJB201704007).

## References

[1] S. W. Liao, W. Yao, X. N. Han, J. Y. Wen, and S. J. Cheng, "Chronological operation simulation framework for regional power system under high penetra-

tion of renewable energy using meteorological data," *Applied Energy*, vol. 203, pp. 816-828, 2017.

[2] Y. Shen, W. Yao, J. Y. Wen, and H. B. He, "Adaptive wide-area power oscillation damper design for photovoltaic plant considering delay compensation," *IET Generation, Transmission & Distribution*, DOI: 10.1049/iet-gtd.2016.2057

[3] A. Gustafsson, M. Saltzer, A. Farkas, H. Ghorbani, T. Quist, and M. Jeroense, "The new 525 kV extruded HVDC cable system," *ABB Grid Systems, Technical Paper*, Aug. 2014.

[4] Y. Shen, W. Yao, J. Y. Wen, H. B. He, and W. B. Chen, "Adaptive supplementary damping control of VSC-HVDC for interarea oscillation using GrHDP," *IEEE Trans. Power Syst.*, DOI: 10.1109/TPWRS.2017.2720262.

[5] N. Flourentzou, V. G. Agelidis, and G. D. Demetriades, "VSC-based HVDC power transmission systems: an overview," *IEEE Trans. Power Electron.*, vol. 24, no. 3, pp. 592-602, Mar. 2009.

[6] A. M. Gole and M. Meisingset, "Capacitor commutated converters for long-cable HVDC transmission," *Power Engineering Journal*, vol. 16, no. 3, pp. 129-134, June 2002.

[7] J. Liang, T. J. Jing, O. G. Bellmunt, J. Ekanayake, and N. Jenkins, "Operation and control of multiterminal HVDC transmission for offshore wind farms," *IEEE Trans. Power Del.*, vol. 26, no. 4, pp. 2596-2604, Oct. 2011.

[8] B. Yang, T. Yu, X. S. Zhang, L. N. Huang, H. C. Shu, and L. Jiang. "Interactive teaching-learning optimizer for parameter tuning of VSC-HVDC systems with offshore wind farm integration," *IET Generation, Transmission & Distribution.* DOI: 10.1049/iet-gtd.2016.1768

[9] S. Li, T. A. Haskew, and L. Xu, "Control of HVDC light system using conventional and direct current vector control approaches," *IEEE Trans. Power Electron.*, vol. 25, no. 12, pp. 3106-3118, Dec. 2010.

[10] S. Y. Ruan, G. J. Li, L. Peng, Y. Z. Sun, and T. T. Lie, "A nonlinear control for enhancing HVDC light transmission system stability," *International Journal of Electrical Power and Energy Systems*, vol. 29, pp. 565-570, 2007.

[11] G. Beccuti, G. Papafotiou, and L. Harnefors, "Multivariable optimal control of HVDC transmission links with network parameter estimation for weak grids," *IEEE Trans. Control Syst. Technol.*, vol. 22, no. 2, pp. 676-689, Mar. 2014.

[12] C. Schmuck, F. Woittennek, A. Gensior, and J. Rudolph, "Feed-forward control of an HVDC power transmission network," *IEEE Trans. Control Syst. Technol.*,

vol. 22, no. 2, pp. 597-606, Mar. 2014.

[13] H. S. Ramadan, H. Siguerdidjane, M. Petit, and R. Kaczmarek, "Performance enhancement and robustness assessment of VSC-HVDC transmission systems controllers under uncertainties," *International Journal of Electrical Power and Energy Systems*, vol. 35, no. 1, pp. 34-46, Dec. 2012.

[14] A. Moharana and P. K. Dash, "Input-output linearization and robust sliding-mode controller for the VSC-HVDC transmission link," *IEEE Trans. Power Del.*, vol. 25, no. 3, pp. 1952-1961, July 2010.

[15] B. Yang, Y. Y. Sang, K. Shi, Wei Yao, L. Jiang, and T. Yu, "Design and real-time implementation of perturbation observer based sliding-mode control for VSC-HVDC systems," *Control Eng. Pract.*, vol. 56, pp. 13-26, 2016.

[16] L. Zhang, L. Harnefors, and H. Nee, "Interconnection of two very weak AC systems by VSC-HVDC links using power-synchronization control," *IEEE Trans. Power Syst.*, vol. 26, no. 1, pp. 344-355, July 2011.

[17] K. Meah and A. H. M. Sadrul Ula, "A new simplified adaptive control scheme for multi-terminal HVDC transmission systems," *International Journal of Electrical Power and Energy Systems*, vol. 32, pp. 243-253, 2010.

[18] N. R. Chaudhuri and B. Chaudhuri, "Adaptive droop control for effective power sharing in multi-terminal DC (MTDC) grids," *IEEE Trans. Power Syst.*, vol. 28, no. 1, pp. 21-29, Feb. 2013.

[19] J. Machowski, P. Kacejko, L. Nogal, and M. Wancerz, "Power system stability enhancement by WAMS-based supplementary control of multi-terminal HVDC networks," *Control Eng. Pract.*, vol. 21, pp. 583-592, 2013.

[20] B. Yang, L. Jiang, Wei Yao, and Q. H. Wu, "Perturbation observer based adaptive passive control for damping improvement of multi-terminal voltage source converter-based high voltage direct current systems," *Transactions of the Institute of Measurement and Control*, vol. 39, no. 9, pp. 1409-1420, 2017.

[21] R. Ortega, A. Schaft, I. Mareels, and B. Maschke, "Putting energy back in control," *IEEE Control Systems*, vol. 21, no. 2, pp. 18-33, 2001.

[22] B. Yang, L. Jiang, Wei Yao, and Q. H. Wu, "Perturbation estimation based coordinated adaptive passive control for multimachine power systems," *Control Eng. Pract.*, vol. 44, pp. 172-192, 2015.

[23] R. Ortega, M. Galaz, A. Astolfi, Y. Z. Sun, and T. L. Shen, "Transient stabilization of multimachine power systems with nontrivial transfer conductances," *IEEE Trans. Autom. Control*, vol. 50, no. 1, pp. 60-75, Jan. 2005.

[24] I. L. Garcia, G. E. Perez, H. Siguerdidjane, and A. D. Cerezo, "On the passivity-based power control of a doubly-fed induction machine" *International Journal of Electrical Power and Energy Systems*, vol. 45, no. 1, pp. 303-312, Feb. 2013.

[25] L. Harnefors, A. G. Yepes, A. Vidal, and J. Doval-Gandoy, "Passivity-based controller design of grid-connected VSCs for prevention of electrical resonance instability," *IEEE Trans. Ind. Electron.*, vol. 62, no. 2, pp. 702-710, Feb. 2015.

[26] F. M. Serra, C. H. De Angelo, and D. G. Forchetti, "Interconnection and damping assignment control of a three-phase front end converter," *International Journal of Electrical Power and Energy Systems*, vol. 560, pp. 317-324, Sep. 2014.

[27] M. Mehrasa, M. E. Adabi, E. Pouresmaeil, and Jafar Adabi, "Passivity-based control technique for integration of DG resources into the power grid," *International Journal of Electrical Power and Energy Systems*, vol. 58, pp. 281-291, Jun. 2014.

[28] N. Fernandopulle and R. T. H. Alden, "Incorporation of detailed HVDC dynamics into transient energy functions," *IEEE Trans. Power Syst.*, vol. 20, no. 2, pp. 1043-1052, May 2005.

[29] X. M. Fan, L. Guan, C. J. Xia, and T. Y. Ji, "IDA-PB control design for VSC-HVDC transmission based on PCHD model," *Int. Trans. Electr. Energ. Syst.*, vol. 25, no. 10, pp. 2133-2143, 2015.

[30] D. Jovcic, "Phase locked loop system for FACTS," *IEEE Trans. Power Syst.*, vol. 18, no. 3, pp. 1116-1124, Aug. 2003.

[31] Y. Chen, J. Dai, G. Damm, and F. Lamnabhi-Lagarrigue, "Nonlinear control design for a multi-terminal VSC-HVDC system," *in 2013 European Control Conference (ECC)*, Zurich, Switzerland, pp. 3536-3541, 17-19 July 2013.

[32] X. P. Zhang, "Multiterminal voltage-source converter-based HVDC models for power flow analysis," *IEEE Trans. Power Syst.*, vol. 19, no. 4, pp. 1877-1884, Oct. 2004.

[33] N. Geddada, M. K. Mishra, and M. V. Kumar, "SRF based current controller using PI and HC regulators for DSTATCOM with SPWM switching," *International Journal of Electrical Power and Energy Systems*, vol. 67, pp. 87-100, May 2015.

[34] A. Isidori, "Nonlinear control systems," Berlin: Springer, 3rd edition, 1995.

[35] W. Yao, L. Jiang, J. Y. Wen, Q. H. Wu, and S. J. Cheng, "Wide-area damping controller of FACTS devices for inter-area oscillations considering communica-

tion time delays," *IEEE Trans. Power Syst.*, vol. 29, no. 1, pp. 318-329, Jan. 2014.

[36] W. Yao, L. Jiang, J. Y. Wen, Q. H. Wu, and S. J. Cheng, "Wide-area damping controller for power system inter-area oscillations: a networked predictive control approach," *IEEE Trans. Control Syst. Tech.*, vol. 23, no. 1, pp. 27-36, Jan, 2015

[37] R. Perveen, N. Kishor, and S. R. Mohanty, "Fault detection and optimal coordination of overcurrent relay in offshore wind farm connected to onshore grid with VSCCHVDC," *International Transactions on Electrical Energy Systems*, vol. 26, no. 4, pp. 841-863, 2016.

[38] M. E. Baran and N. R. Mahajan, "Overcurrent protection on voltage-source-converter-based multiterminal DC distribution systems," *IEEE Transactions on Power Delivery*, vol. 22, pp. 406-412, 2007.

[39] S. L. Blond, R. B. Jr, D. V. Coury, and J. C. M. Vieira, "Design of protection schemes for multi-terminal HVDC systems," *Renewable and Sustainable Energy Reviews*, vol. 56, pp. 965-974, 2016.

[40] L. Tang and B. T. Ooi, "Locating and isolating DC faults in multiterminal DC systems," *IEEE Trans. Power Del.*, vol. 22, no. 3, pp. 1877-1884, Jul. 2007.

[41] J. Liu, J. Y. Wen, W. Yao, Y. Long. "Solution to short-term frequency response of wind farms by using energy storage systems," *IET Renewable Power Generation*, vol. 10, no. 5, pp. 669-678, 2016.

[42] B. Yang, L. Jiang, L. Wang, W. Yao, and Q. H. Wu. "Nonlinear maximum power point tracking control and modal analysis of DFIG based wind turbine," *International Journal of Electrical Power and Energy Systems*, vol. 74, pp. 429-436, 2016.

[43] B. Yang, X. S. Zhang, T. Yu, H. C. Shu, and Z. H. Fang. "Grouped grey wolf optimizer for maximum power point tracking of doubly-fed induction generator based wind turbine," *Energy Conversion and Management*, vol. 133, pp. 427-443, 2017.

[44] B. Yang, T. Yu, H. C. Shu, J. Dong, and L. Jiang. "Robust sliding-mode control of wind energy conversion systems for optimal power extraction via nonlinear perturbation observers," *Applied Energy*, http://dx.doi.org/10.1016/j.apenergy.2017.08.027

[45] B. Yang, Y. L. Hu, H. Y. Huang, H. C. Shu, T. Yu, and L. Jiang. "Perturbation estimation based robust state feedback control for grid connected DFIG wind

energy conversion system," *International Journal of Hydrogen Energy*, vol. 42, no. 33, pp. 20994-21005, 2017.

[46] C. Y. Guo and C. Y. Zhao, "Supply of an entirely passive AC network through a double-infeed HVDC system," *IEEE Trans. Power Electron.*, vol. 24, no. 11, pp. 2835-2841, Nov. 2010.

[47] C. Zheng, X. X. Zhou and R. M. Li, "Dynamic modeling and transient simulation for VSC based HVDC in multi-machine system," *2006 International Conference on Power System Technology*, Chongqing, 2006, pp. 1-7.

[48] W. Chen, X. Zhu, L. Z. Yao, G. F. Ning, Y. Li, Z. B. Wang, W. Gu, and X. H. Qu, "A novel interline DC power flow controller (IDCPFC) for meshed HVDC grids," *IEEE Trans. Power Del.*, vol. 31, no. 4, pp. 1719-1727. 2016.